Energy Conversion and Management 239 (2021) 114215

Contents lists available at ScienceDirect

Energy Conversion and Management

journal homepage: www.elsevier.com/locate/enconman

# Performance assessment of solar PV-driven hybrid HDH-RO desalination system integrated with energy recovery units and solar collectors: Theoretical approach

Mohamed Abdelgaied [a], A.E. Kabeel [a,b,*], A.W. Kandeal [c,d], H.F. Abosheiasha [e], S.M. Shalaby [e], Mofreh H. Hamed [d,f], Nuo Yang [c,*], Swellam W. Sharshir [c,d]

[a] Mechanical Power Engineering Department, Faculty of Engineering, Tanta University, Tanta, Egypt
[b] Faculty of Engineering, Delta University for Science and Technology, Gamasa, Egypt
[c] State Key Laboratory of Coal Combustion, Huazhong University of Science and Technology, Wuhan 430074, China
[d] Mechanical Engineering Department, Faculty of Engineering, Kafrelsheikh University, Kafrelsheikh 33516, Egypt
[e] Engineering Physics and Mathematics Department, Faculty of Engineering, Tanta University, Egypt
[f] Higher Institute of Engineering and Technology, MNF-HIET, Menoufia, Egypt

ARTICLE INFO

*Keywords:*
Desalination
Reverse osmosis
Humidification-dehumidification
Photovoltaics
Specific power consumption
Solar energy

ABSTRACT

Recently, constructing a high productive desalination unit with low power consumption has been a challenge. Along with that, this study aimed to simulate a new hybrid desalination unit merging two common techniques of high freshwater production: humidification-dehumidification (HDH), and reverse osmosis (RO). For low power consumption, the hybrid HDH-RO unit was powered with a photovoltaic (PV) systems. The system was provided with thermal energy recovery (TER) units, double-pass solar air collectors (SACs), and evacuated tube solar water collectors (SWCs). The TER units were parallel connected to the backside of PV panels for dual function: enhancing the PV conversion performance by cooling and preheating the seawater before entering the SWC. Both SAC and SWC were proposed to improve the evaporation rate inside the humidifier of the HDH unit. For a comprehensive analysis of the HDH-RO system, five coupled theoretical models were derived and solved, which all were validated by previous experimental data from the literature. All results confirmed that the proposed system can be a good choice for producing freshwater with low power consumption. The maximum hourly freshwater production of the new hybrid HDH-RO desalination system varied between 192 and 200 L, with a water recovery ratio ranged between 48 and 49.8%. Also, its specific power consumption (SPC) ranged between 1.22 and 1.24 kWh/m$^3$, with an average saving a range between 14.7 and 65% compared to previous techniques of RO desalination system.

## 1. Introduction

Based on the sustainable development agenda, having safe and accessible water for everyone is an essential part of the world we want to live in. Energy and water are important sources because they are linked together. The worldwide population explosion and rapid industrial growth have increased the demand for clean water. To achieve sustainable development goals, technological development in the field of desalination with renewable energies is urgently required. Among the various sources of renewable energy (solar, wind, and geothermal energies), and since solar energy is available in high density in the Middle East region, it is therefore used effectively in the field of desalination.

The humidification-dehumidification (HDH) desalination process represents one of the most important and promising desalination technologies. The freshwater production rate of HDH desalination technology is highly dependent on the temperature of the air and water entering to the humidifier as well as the water–air flow ratio. Nafey et al. [1] theoretically evaluated the influences of operating conditions on HDH desalination productivity. They found that the water-mass ratio, cooling water flow rate, and intensity of solar radiation had a strong effect on the productivity of HDH desalination unit. Lavasani et al. [2] empirically studied the productivity of the HDH desalination unit. Zubair [3] examined the optimal water–air ratio achieve the highest freshwater production rate of the solar HDH desalination system. Rajaseenivasan

* Corresponding authors at: Mechanical Power Engineering Department, Faculty of Engineering, Tanta University, Tanta, Egypt (A.E. Kabeel).
*E-mail addresses:* kabeel@hotmail.com (A.E. Kabeel), nuo@hust.edu.cn (N. Yang).

https://doi.org/10.1016/j.enconman.2021.114215
Received 14 February 2021; Accepted 22 April 2021

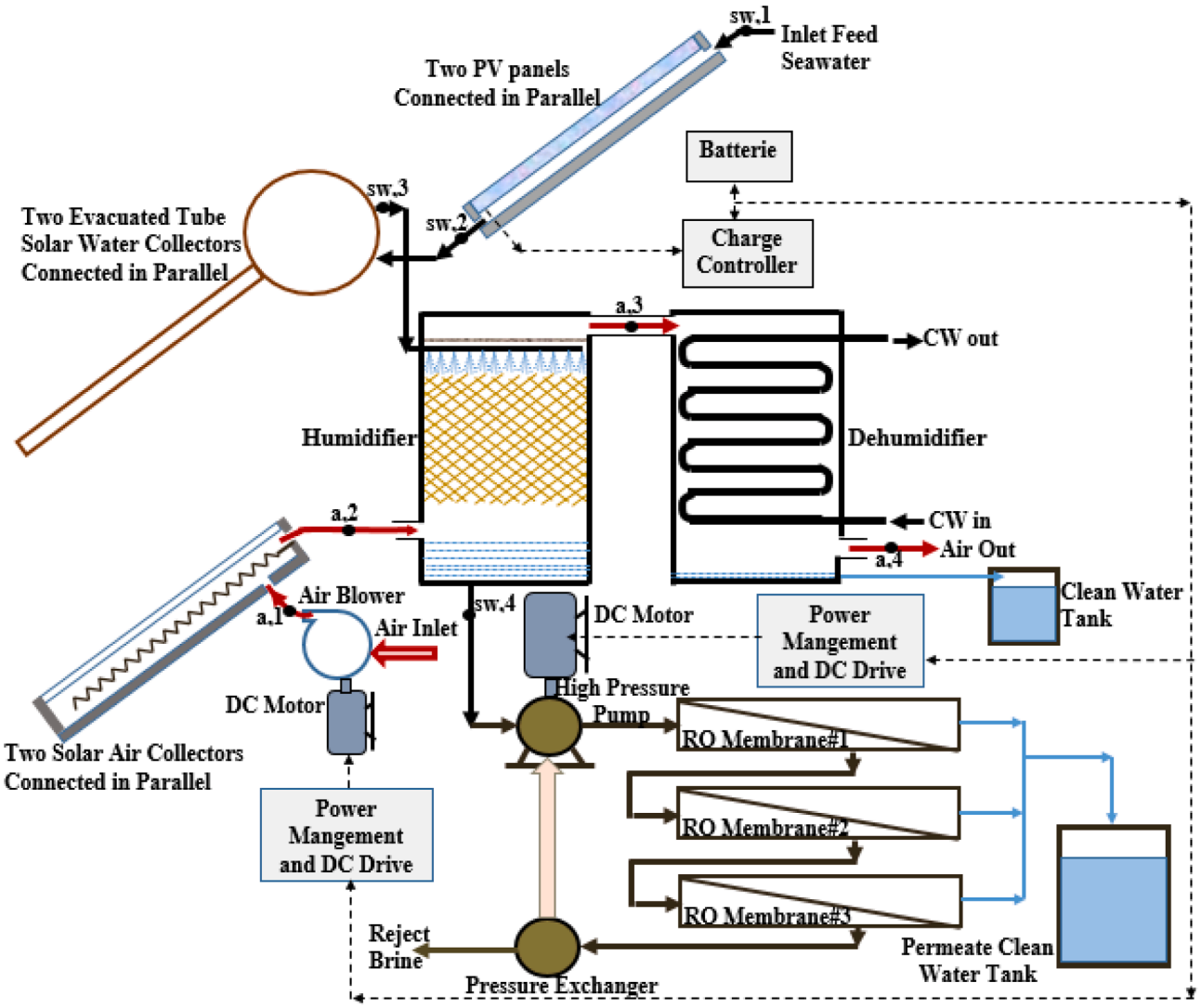


**Fig. 1.** A schematic diagram of the proposed hybrid HDH-RO desalination system.

and Srithar [4] empirically investigated the performance of HDH desalination unit integrated with a dual-purpose solar collector. Ghalavand et al. [5] examined the influences of operating conditions of the humidifier on a freshwater production of solar assisted HDH desalination unit.

Photovoltaic (PV) solar panels are nowadays widely used to generate electricity [6,7]. A cooling medium such as air or water can be used to cool the PV panels, recover heat and improve the conversion efficiency [8]. The recovered heat can also be used as a driver for desalination processes, providing an excellent option that contributes to a sustainable environment. Where electricity and thermal energy can be jointly generated through hybrid photovoltaic/thermal (PV/T) units. Wang et al. [9] studied the performance of the cooled PV modules integrated with HDH desalination (PV-HDH) unit. They also examined the influences of the convection mode and process temperature on freshwater productivity. Giwa et al. [10] conducted the influences of the environmental effect on the performance of PV-HDH system with thermal energy recovery (TES) technology. Gabrielli et al. [11] studied the impact of design and operating conditions on the behavior of HDH desalination unit integrated with PV/T modules. To enhance the generating freshwater and electricity, simultaneously this was done by utilizing the concentrating solar collector [12]. Rafiei et al. [13] theoretically studied the influences of operating conditions on the freshwater production of the HDH desalination system integrated with solar dish concentrator and PV/T system. Mahmoud et al. [14] theoretically assessed the behavior of a hybrid solar distiller/HDH desalination system integrated with PV panels and solar concentrators.

The reverse osmosis (RO) membrane process is widely used in seawater desalination as it is characterized by easy operation in the long term as well as low energy consumption [15]. While it is still highly required to reduce the energy consumption rates of the RO process and make it an available technology for most of the global region [16–19]. Recently, in order to reduce the energy consumption of reverse osmosis systems, pressure retarded osmosis (PRO) has been used. The PRO can recover energy from RO brine to supplement the RO process with the aim of reducing the electricity consumption rate in the high-pressure pump [20–23]. Karimi et al. [24] empirically studied the behavior of RO desalination system driven by PV panels. Bargiacchi et al. [25] reduced the power consumption rate in RO desalination plant by combining the PRO with RO plant. Ahmad et al. [26] analytically studied the performance of hybrid photovoltaic/reverse osmosis (PV/RO) desalination plant driving by PV panels. Cerva et al. [27] utilized reverse electrodialysis (RED) in order to reduce the power consumption rate in RO desalination plant. Alsarayreh et al. [28] studied the performance of various membranes utilized in RO desalination plants. Generally, membrane technologies have been widely used to extract important energy elements, such as lithium, via selecting a proper membrane like that having 2D subnanometer channel [29].

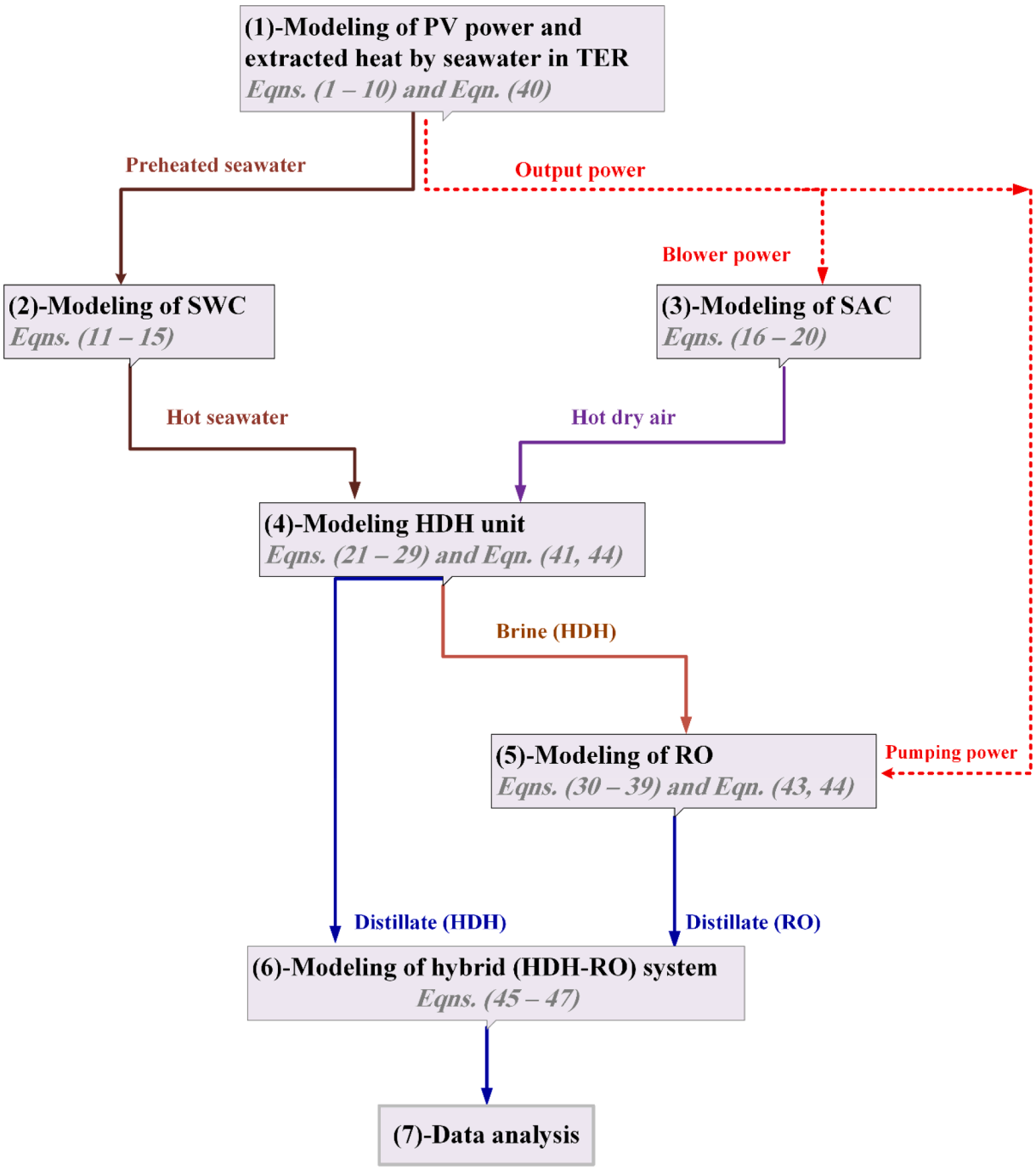


**Fig. 2.** Flow chart representation of proposed hybrid HDH-RO desalination system.

Based on the literature, developing a new hybrid system to desalinate seawater with lower power consumption remains a challenging issue and promising way. Along with that, the current work aimed to develop a new hybrid system, humidification-dehumidification-reverse osmosis (HDH-RO), that can desalinate the seawater at lower energy consumption rates than a separate RO desalination system. That system was considered to be a good choice for remote regions. To achieve this vision, this new proposed HDH-RO desalination system was suggested to be integrated with PV panels, for power generation, with thermal energy recovery (TER) system, evacuated tube solar collector (SWC), and solar air collector (SAC). For comprehensive performance evaluation of this system, five coupled models were derived, and each model was validated by the previous experimental data.

## 2. The proposed hybrid desalination system configuration

A schematic diagram of the proposed hybrid HDH-RO desalination system operated by fixed PV panels with thermal energy recovery (TER) system and solar thermal collectors is shown in Fig. 1. In addition, the process flow chart within the system is schematically presented in Fig. 2. The proposed hybrid HDH-RO system consisted of five sections: PV panels, evacuated tube solar water collector (SWC), solar air collector (SAC), HDH desalination unit, and RO desalination system. Two PV panels was used to obtain the required electricity to drive the air blower and high-pressure pump. The panels were attached in parallel with TER unit, that was utilized to pre-heat the seawater before feeding into the evacuated solar collector besides cooling the panels to enhance their conversion performance. Also, the PV system contained the charge

controllers, batteries, and DC drive. Two evacuated tube SWCs, connected in parallel, and two SACs (double-pass with v-corrugated absorber), connected in parallel, were utilized to heat the seawater, and air, respectively, before entering to the humidifier of HDH desalination unit, to improve the evaporation rate. The HDH desalination unit is comprised of a humidifier and dehumidifier. The outlet brine water, leaving the humidifier, was being fed into the RO unit. RO unit consists of a high-pressure pump, three spiral wound membrane modules connected in series, and a pressure exchanger as an energy recovery device.

The specifications and the mathematical model of each component are presented below:

### 2.1. Modelling of PV panel cooling (seawater preheater)

A back channel was attached to each PV module, through which cold seawater was flowing in order to cool the PV panel, by extracting heat from its back face, and at the same time this stage represented the preheating stage of the seawater.

The various temperatures of the PV module can be calculated as following [13]:

Backside surface temperature of PV module is given as:

$$T_{bs} = \frac{h_{p1}(\alpha\tau)_{eff} I(t) + U_{tT} T_a + h_T T_w}{U_{tT} + h_T} \tag{1}$$

PV module cell temperature is given as:

$$T_C = \frac{\tau_G[\alpha_C \beta_C + \alpha_T(1-\beta_C)]I(t) - \eta_C I(t)\beta_C + U_t T_a + U_T T_{bs}}{U_t + U_T} \tag{2}$$

Electrical efficiency of PV module:

$$\eta_C = \eta_o[1 - 0.0045(T_C - 298.15)] \tag{3}$$

The outlet temperature of seawater flowing under the PV modules can be calculated using:

$$T_{sw2} = \left[\frac{h_{p1}h_{p2}(\alpha\tau)_{eff} I(t)}{U_L} + T_a\right]\left[1 - \exp\left(-\frac{F^{'} A_C U_L}{mC_p}\right)\right] + T_{sw1}\exp\left(-\frac{F^{'} A_C U_L}{mC_p}\right) \tag{4}$$

where;

$$(\alpha\tau)_{eff} = \tau_G\{\beta_C + \alpha_T(1-\beta_C) - \eta_C\beta_C\} \tag{5}$$

The coefficient of overall heat transfer from the PV module to the surrounding on the backside, W/m$^2$ K.

$$U_L = U_{tw} + U_b \tag{6}$$

The coefficient of overall heat transfer from the front glass of the PV module to water, W/m$^2$ K.

$$U_{tw} = \left[\frac{1}{U_{tT}} + \frac{1}{hi}\right]^{-1} \tag{7}$$

The coefficient of overall heat transfer from water to the surrounding, W/m$^2$ K.

$$U_b = \left[\frac{L_i}{k_i} + \frac{1}{hi}\right]^{-1} \tag{8}$$

The coefficient of overall heat transfer $U_{tT}$ from glass cover to glass plate of PV module, W/m$^2$ K.

$$U_{tT} = \frac{(U_T \times h_T)}{(U_T + h_T)} \tag{9}$$

The coefficient of conductive heat transfer from PV cells to water flows through the glass plate, W/m$^2$ K.

$$U_T = \left[\left(\frac{L_g}{k_g}\right) + \left(\frac{1}{h_{o(i)}}\right)\right]^{-1} \tag{10}$$

and, F′ is the view factor; $h_{p1}$ is the glass cover penalty factor = 0.8772; $h_{p2}$ is the glass plate penalty factor = 0.9841; $L_g$ is the PV module glass thickness = 0.003 m; $k_g$ is the glass thermal conductivity of PV module = 1 W/m K; $h_i$ is the heat transfer cofficient of insulation = 5.8 W/m$^2$ K; ki insulation thermal conductivity = 0.035 W/m K; $L_i$ insulation thickness = 0.05 m; $h_T$ is the tedlar heat transfer cofficient from back surface to air = 500 W/m$^2$ K; $\alpha_c$ is the solar cell absorptivity = 0.9; $\alpha_g$ is the glass plate absorptivity = 0.8; $\beta_c$ is the solar cell packing factor = 0.83; $\tau_g$ is the PV module glass cover transmittivity = 0.95; and $\eta_o$ is the reference PV module efficiency = 15%.

### 2.2. Modelling of evacuated tube solar water collector (SWC)

The total heat absorbed by the evacuated tubes ($\dot{Q}_{total}$) can be calculated as follows [30,31]:

$$\dot{Q}_{total} = \dot{Q}_u + \dot{Q}_{loss} = D_{abs} \times L \times N \times \alpha_{abs} \times \tau_g \times DNI \tag{11}$$

The seawater temperature at the outlet from the tubules of the collector can be calculated as follows:

$$T_{sw,3} = T_{sw,2} + \frac{\dot{Q}_u}{\dot{m}_{sw} \times C_p} = T_{sw,2} + \frac{\dot{Q}_{total} - \dot{Q}_{loss}}{\dot{m}_{sw} \times C_p} \tag{12}$$

The total heat loss ($\dot{Q}_{loss}$) from the evacuated tube collector to the environment can be written as follows:

$$\dot{Q}_{loss} = \pi D_{abs} \times L \times N \times \left[h_{abs-g}(T_{abs} - T_a) + \sigma\varepsilon_{abs}\left(T^4_{abs} - T^4_s\right)\right] \tag{13}$$

where; DNI is the direct normal solar radiation (W/m$^2$); $h_{abs\text{-}g}$ is the coefficient of convective heat transfer between the absorber and outer glass tube = 0.0001115 W/m$^2$ K; σ is the Stefan-Boltzmann constant = 5.67* 10$^{-8}$ W/m$^2$ K$^4$; εabs is the emissivity of the absorber tube; $T_s$ is the sky temperature; L is the tube length = 1.8 m; $D_{abs}$ is the diameter of absorber tube = 0.047 m; N is the number of tube = 14; $\alpha_{abs}$ is the absorptivity of slective coating = 0.96; and $\tau_g$ is the transmissivity of outer glass tube = 0.96.

$$T_s = 0.0552T_a^{\frac{3}{2}} \tag{14}$$

$$\varepsilon_{abs} = 0.062 + 2 \times 10^{-7}(T_{abs} - 273.15)^2 \tag{15}$$

### 2.3. Modelling of solar air collector (SAC)

The total heat absorbed by the SAC ($\dot{Q}_{total}$) can be calculated as followings [32–34]:

$$\dot{Q}_{total} = \dot{Q}_u + \dot{Q}_{loss} = A_c F_R(\alpha_p\tau_g)DNI \tag{16}$$

The energy loss ($\dot{Q}_{loss}$) from the SAC to the environment is calculated as follows:

$$\dot{Q}_{loss} = A_c F_R U_{loss}(T_{abs} - T_a) \tag{17}$$

The useful heat removed by the SAC can be determined as follows:

$$\dot{Q}_u = \dot{m}_a C_{pa}\left(T_{a,2} - T_{a,1}\right) = A_c F_R[DNI(\tau\alpha) - U_{loss}(T_{abs} - T_a)] \tag{18}$$

The air temperature at the outlet from the SAC is calculated as follows:

$$T_{a,2} = T_{a,1} + \frac{A_c F_R[DNI(\tau\alpha) - U_{loss}(T_{abs} - T_a)]}{\dot{m}_a C_{pa}} \tag{19}$$

The collector heat removal factor is calculated as follows:

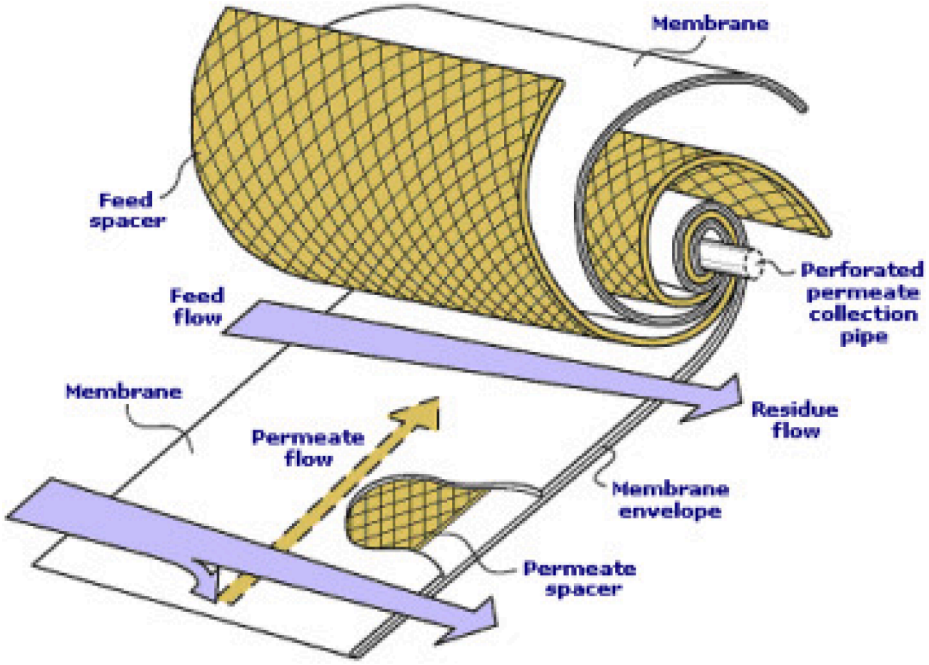


**Fig. 3.** Schematic of spiral wound membrane module [26].

$$F_R = \frac{\dot{m}_a C_{pa}}{A_c U_{loss}} \left\{ 1 - exp\left[ \frac{U_{loss} F^{'} A_c}{\dot{m}_a C_{pa}} \right] \right\} \tag{20}$$

where; $U_{loss}$ is the total loss coefficient = 4.30 W/m$^2$ K; F' is the collector efficiency factor = 0.984; and $\alpha\tau$ = 0.850

### 2.4. Modelling of Humidification-Dehumidification (HDH) desalination unit

As generally known, the HDH unit consists of two interconnected towers: Humidifier and dehumidifier, as shown in Fig. 1. Inside the humidifier or evaporator, the hot water is being sprayed through sprayers over a suitable packing material which should have a high surface area to volume ratio. The hot dry air is being blown from the downside of the evaporator through the packing material to hold as much as possible of vapor (i.e., being humidified). Then the humid air enters the shell side of the condenser (dehumidifier) rejecting heat to the cooling water, that flows in the tube side. Hence, the condensate is being collected (as freshwater). For this process, the energy and mass balance equations for each component (humidifier and dehumidifier), are given as follows [10,13,35]:

Humidifier:

$$\dot{m}_{sw} h_{sw3} + \dot{m}_a h_{a2} = \dot{m}_{bw} h_{bw4} + \dot{m}_a h_{a3} \tag{21}$$

$$\dot{m}_{bw} = \dot{m}_{sw} - \dot{m}_{fw} \tag{22}$$

Dehumidifier:

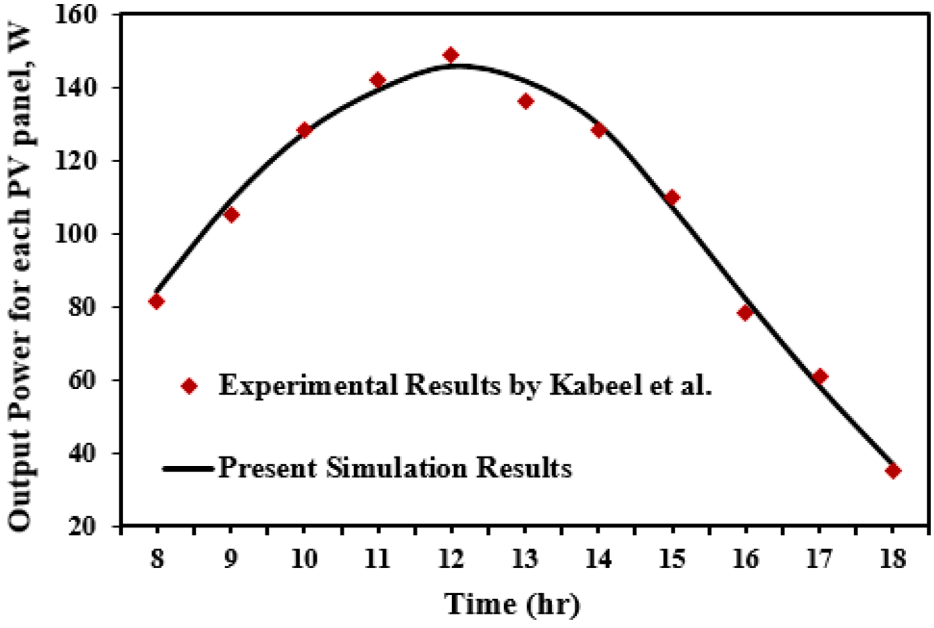


**Fig. 4.** Comparison between the present simulation results of the PV output power and the experimental results reported by Kabeel et al. [36].

$$\dot{m}_{cw}\left(h_{cw,o}-h_{cw,i}\right)+\dot{m}_{fw}h_{fw}=\dot{m}_a(h_{a3}-h_{a4}) \tag{23}$$

$$\dot{m}_{fw}=\dot{m}_{da}(\omega_{a3}-\omega_{a4}) \tag{24}$$

$$\dot{m}_{da}=\frac{\dot{m}_a}{(1+\omega_{a2})} \tag{25}$$

Air specific enthalpy:

$$h_{a,i}=1.006T_{a,i}+\omega_{a,i}\left(2501+1.86T_{a,i}\right) \tag{26}$$

The saturated liquid water specific enthalpy in the temperature range (0.01–150 °C) is calculated as:

$$h_{w,i}=d_1+d_2T_{w,i}+d_3T^2{}_{w,i}+d_4T^3{}_{w,i}+d_5T^4{}_{w,i}+d_6T^5{}_{w,i} \tag{27}$$

where; $d_1=-2.844699\times10^{-2}$, $d_2=4.211925$, $d_3=-1.017034\times10^{-3}$, $d_4=1.311054\times10^{-5}$, $d_5=-6.756469\times10^{-8}$, $d_6=1.724481\times10^{-10}$.

Air humidity ratio:

$$\omega_{a,i}=\frac{0.622\times P_{s,i}}{P_{air,i}}=\frac{0.622P_{s,i}}{P_a-P_{s,i}} \tag{28}$$

Air vapor pressure:

$$P_{s,i}=RH_{a,i}\times\frac{e^{\left[(77.3450+(0.0057T_{a,i}))-\left(\frac{7235}{T_{a,i}}\right)\right]}}{T_{a,i}{}^{8.2}} \tag{29}$$

### 2.5. Modelling of reverse osmosis (RO) unit

In the present study, three stages of spiral wound membranes connected in series are proposed in RO desalination system. In the first edge of membranes, seawater is forced with high pressure into the feed channels. In the second end of the membrane, the brine water feed to the second stage of the membrane and so on. During the filtration process, the clean water flows within polyamide active layers into the permeate channel. The high concentration brine out from the third stage are flowing into the pressure exchanger (energy recovery) and rejected after this. Fig. 3 shows the schematic of spiral wound membranes.Fig. 4

The permeate flow rate is estimated by Equation [26]:

$$Q_p=A_{perm}\ S_e\ (TCF)(FF)\left[\left(P_f-\frac{\Delta P_{fc}}{2}-P_p\right)-\left(CPF\frac{\pi_f+\pi_b}{2}-\pi_p\right)\right] \tag{30}$$

where $Q_p$ is permeating flow rate ($m^3/h$); $A_{perm}$ is the clean water permeability = $1.086\times10^{-5}$ $m^3/m^2$ h bar; $S_e$ is the active area of membrane = 1.2 $m^2$; FF is the membrane fouling factor; TCF is the temperature correction factor; $P_f$ is the seawater feed pressure = 41 bar; $\Delta P_{fc}$ is the pressure drop = 1 bar; $P_p$ is the permeate pressure = 1 bar; CPF is the concentration polarization factor; and π is the osmotic pressure (bar).

The temperature correction factor (TCF) is estimated by the following equation [26]:

$$TCF=\left\{\begin{array}{l} exp\left[2640\left(\frac{1}{198}-\frac{1}{T_{sw}+273.15}\right)\right], T_{sw}\geqslant25^{\circ}C \\ exp\left[3020\left(\frac{1}{198}-\frac{1}{T_{sw}+273.15}\right)\right], T_{sw}<25^{\circ}C \end{array}\right\} \tag{31}$$

The concentration polarization factor (CPF) is estimated by the following equation [26]:

$$CPF=e^{0.7Y} \tag{32}$$

where; Y is a recovery ratio and is calculated as follows [26]:

$$Y=\frac{Permeate\ \ flow\ \ rate}{Feed\ \ flow\ \ rate}=\frac{Q_p}{Q_f} \tag{33}$$

The osmotic pressure (π) is calculated as follows [26]:

$$\pi=\left\{\begin{array}{l} \frac{C(T_w+320)}{491000}, C<20000\frac{mg}{l} \\ \frac{0.0117C-34}{14.23}.\frac{(T+320)}{345}, C>20000mg/l \end{array}\right\}bars \tag{34}$$

where; C is the salinity (mg/l or PPM), the salt concentration in the permeate water ($C_p$) is calculated as follows [26]:

$$C_p=B_{salt}S_e(TCF)\left[CPF\left(\frac{C_{fc}}{Q_p}\right)\right] \tag{35}$$

where; $B_{salt}$ is the salt permeability = $4.65\times10^{-7}$ $m^3/m^2$ h, and $C_{fc}$ is the average salt concentration on the concentrate side and is calculated as follows [26]:

$$C_{fc}=\frac{C_f+C_c}{2}=C_f\ln\left(\frac{1}{1-Y}\right)/Y \tag{36}$$

The mass and concentration balance of RO unit is calculated as [26]:

$$Q_f=Q_p+Q_c \tag{37}$$

$$C_fQ_f=C_pQ_p+C_cQ_c \tag{38}$$

The power consumption in high-pressure pump ($\dot{P}_{HPP}$) is calculated as [26]:

$$\dot{P}_{HPP}=\frac{Q_fP_f}{\eta_{HPP}}-Q_CP_c\eta_{ERD} \tag{39}$$

where $\eta_{HPP}$ is the high-pressure pump efficiency = 75%, and $\eta_{ERD}$ is the efficiency of energy recovery device = 80% [26]. The RO membrane model is (SW30-2521); active layer material made from polyamide thin-film composite; membrane length 533 mm and diameter 61 mm; and maximum operating temperature 55 °C.

The mathematical models of the five components of the proposed hybrid were solved by Engineering Equation Solver (EES) which uses the iterative numerical procedure for solving the aforementioned set of equations. To solve the simulation models, the meteorological data were taken from the Meteonorm program for the cairo city, Egypt.

## 3. System performance

### 3.1. PV panels

Herein, the proposed system, two PV panels, connected in series, were utilized to produced the electricity required to operate the present hybrid desalination system. The output power produced from each PV panels $P_m$ can be calculated by the following equation [24]:

$$P_m=4\times P_{m,STC}\left(\frac{DNI}{DNI_{STC}}\right)\left[1-\alpha_p\left(T_c-T_{c,STC}\right)\right] \tag{40}$$

where; $P_{m,STC}$ is the peak power at standared test condition = 180 W; $DNI_{STC}$ is the direct normal solar radiation at standared test condition = 1000 $W/m^2$; $\alpha_p$ is the power temperature coefficient = −0.38%/K; and $T_c$,STC is the cell temperature at standared test condition = 25 °C.

### 3.2. HDH desalination unit

The freshwater productivity $\dot{m}_{fw}$ of HDH desalination unit is defined as:

$$\dot{m}_{fw}=\dot{m}_{da}(\omega_{a3}-\omega_{a4}) \tag{41}$$

The recovery ratio of the HDH desalination unit $RR_{HDH}$ is defined as the ratio between mass flow rate of freshwater produced to the mass flow rate of feed seawater which is given by following equation:

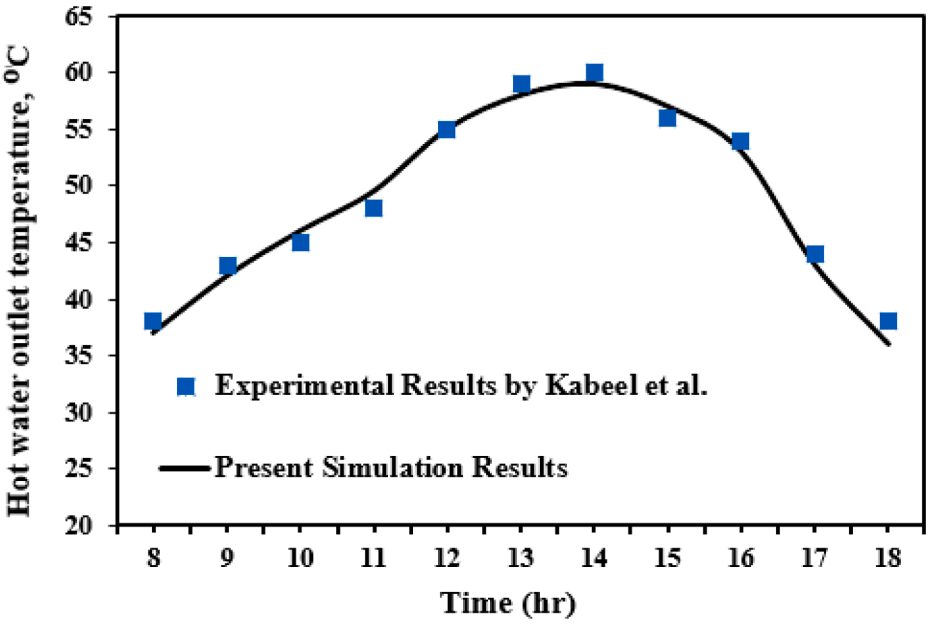


**Fig. 5.** Comparison between the hot water temperature predicted from the theoretical model with the experimental results reported by Kabeel et al. [37].

$$RR_{HDH} = \frac{\dot{m}_{fw}}{\dot{m}_{sw}} \tag{42}$$

### 3.3. RO water desalination system

The permeate flow rate of the RO water desalination system $Q_p$ is estimated by the following equation [26]:

$$Q_p = A_{perm}\ S_e\ (TCF)(FF)\left[\left(P_f - \frac{\Delta P_{fc}}{2} - P_p\right) - \left(CPF\frac{\pi_f + \pi_b}{2} - \pi_p\right)\right] \tag{43}$$

The recovery ratio of the RO water desalination system $RR_{RO}$ is calculated as follows [26]:

$$RR_{RO} = \frac{Permeateflowrate}{Feedflowrate} = \frac{Q_p}{Q_f} \tag{44}$$

### 3.4. Hybrid system of HDH-RO water desalination system

The total freshwater productivity from the hybrid HDH-RO desalination system $Q_{t,fw}$ is defined as;

$$Q_{t,fw} = \left(\dot{m}_{fw} \times \nu_{fw}\right) + Q_p \tag{45}$$

The recovery ratio of the hybrid HDH-RO desalination system $RR_{HDH\text{-}RO}$ is defined as;

$$RR_{HDH-RO} = \frac{\dot{m}_{fw} + Q_p \times \rho_p}{\dot{m}_{sw}} \tag{46}$$

Specific power consumption of the proposed hybrid HDH-RO desalination system ($SPC_{HDH\text{-}RO}$) is defined as:

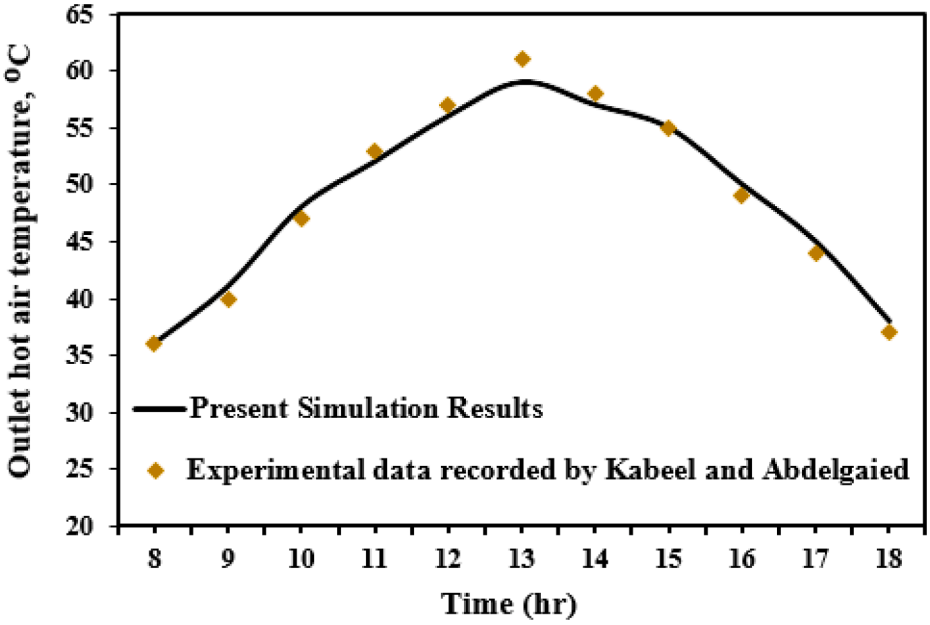


**Fig. 6.** Comparison the outlet hot air temperature predicted from the theoretical model with the experimental data recorded by Kabeel and Abdelgaied [38].

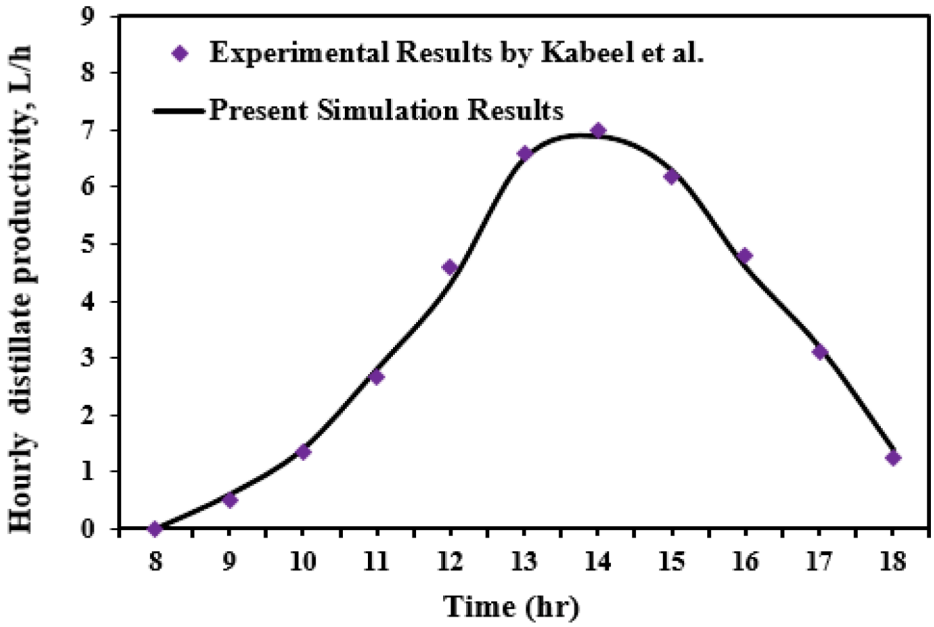


**Fig. 7.** Comparison the hourly productivity predicted from the theoretical model of HDH desalination unit with the experimental data recorded by Kabeel et al. [39].

$$SPC_{HDH-RO} = \frac{\text{Powerconsumption}}{Q_{t,fw}}, kWh/m^3 \quad (47)$$

## 4. Validation of the developed model

To demonstrate the accuracy of the developed numerical model, it was validated by previous experimental data.

### 4.1. Photovoltaic (PV) modeling

The results predicted from the theoretical model of the PV modules was validated through a comparison with the experimental results of Kabeel et al. [36]. Fig. 4 shows that the experimental results for generated power are well in agreement with that was expected from the model under the same climate operating conditions, with an average deviation of 1.83%.

### 4.2. Evacuated tube solar water collector (SWC) modeling

The results of hot water temperature predicted from the theoretical model of the evacuated tube solar collector was validated through a comparison with the experimental results of Kabeel et al. [37]. The model results showed good agreement with that of the experiments, as shown in Fig. 5, with an average deviation reached 2.23%.

### 4.3. Solar air collector (SAC) modeling

The temperature of hot outlet air from the solar air collector predicted from the theoretical model was validated through a comparison with the experimental results of Kabeel et al. [38]. The model resulted

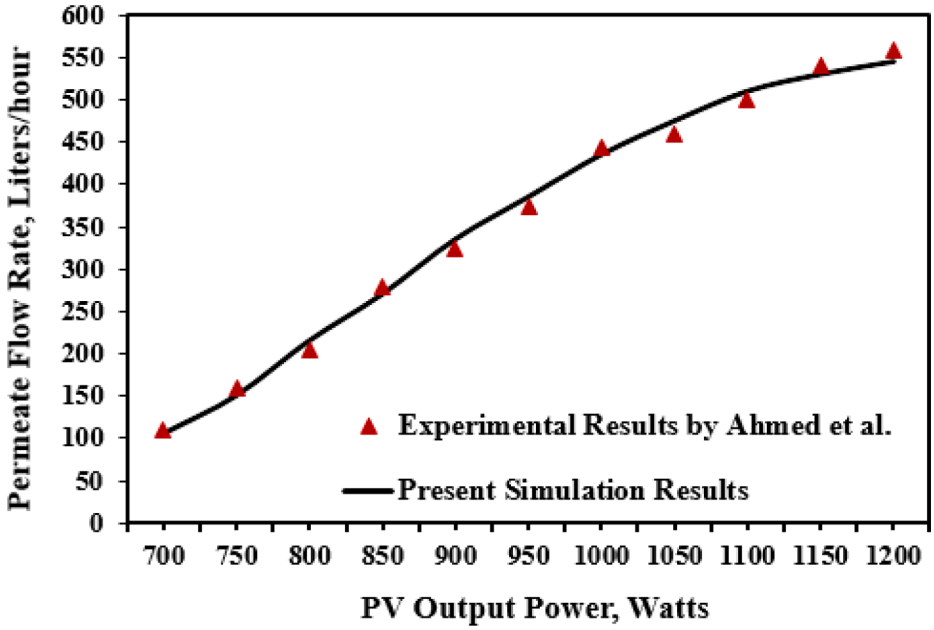


**Fig. 8.** Permeate flow rate of the spiral wound membranes predicted from the theoretical model and experimental results recorded by Ahmed et al. [26].

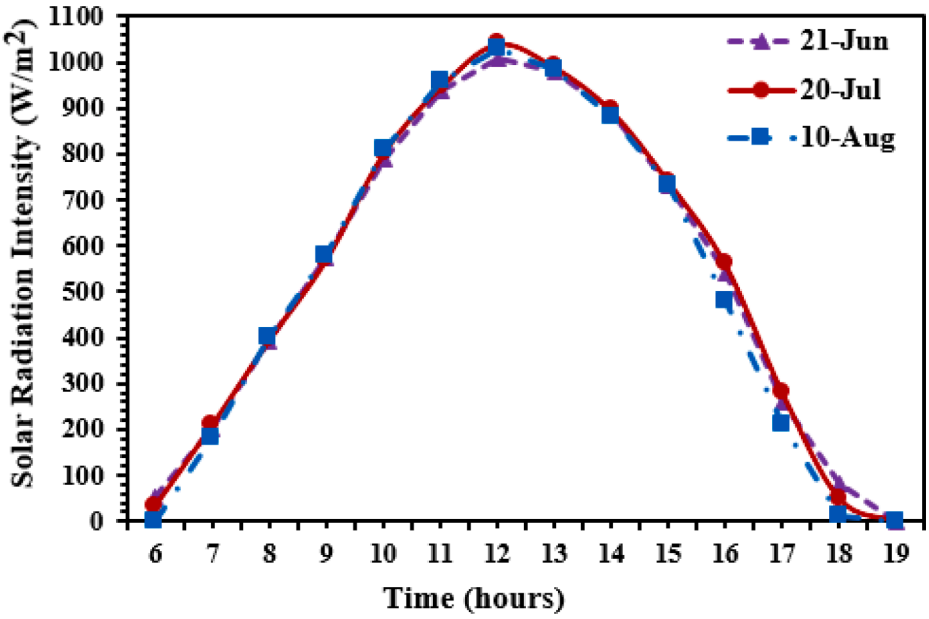


**Fig. 9.** Instantaneous irradiation for the three different days of the year under the Egyptian climate conditions.

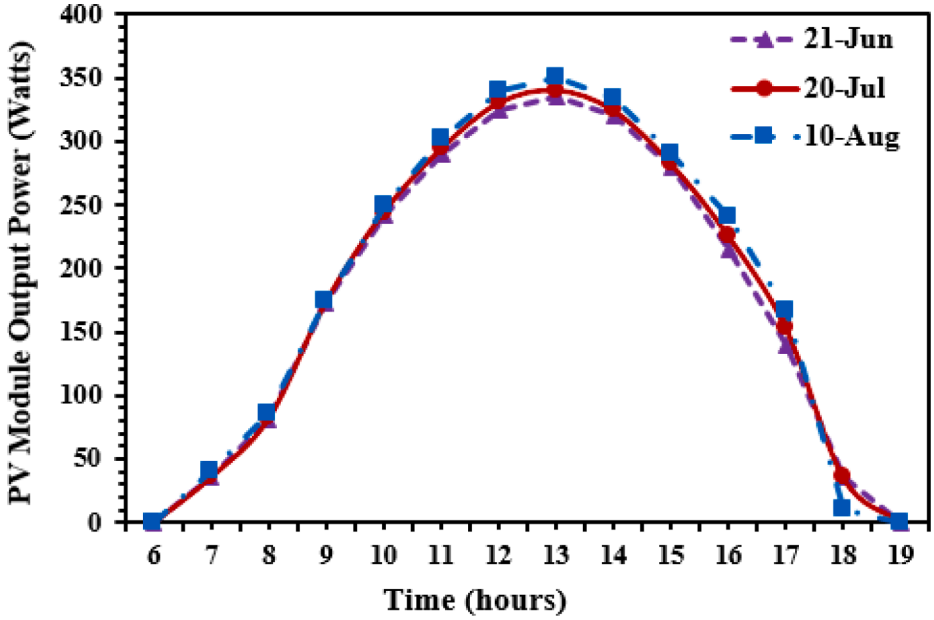


**Fig. 10.** The instantaneous output power produced from the PV panels during three different days.

from data were in a good agreement with the experimental data recorded under the same operating conditions, as shown in Fig. 6, with an average deviation of 1.85% .

### *4.4. Humidification-Dehumidification (HDH) desalination modeling*

The hourly productivity predicted from the theoretical model of the HDH desalination unit was validated through a comparison with the experimental data recorded by Kabeel et al. [39]. The theoretical data were in a good agreement with the experimental data recorded at the same operating conditions, as presented in Fig. 7, with an average deviation reached 2.86%.

### *4.5. Reverse osmosis (RO) modelling*

Fig. 8 shows the permeate flow rate through the spiral wound membranes predicted from the current theoretical model of the RO water desalination system and experimental data recorded by Ahmed et al. [26]. Regarding the same operating conditions, the figure shows a good agreement between the theoretical and experimental data with an average deviation of 3.37%.

## 5. Results and discussion

To analyze the output power produced from the PV panels, their performances were theoretically studied for three different days (21 June, 20 July, and 10 August, under the Egyptian climate conditions, with the solar radiation intensities shown in Fig. 9. The radiation

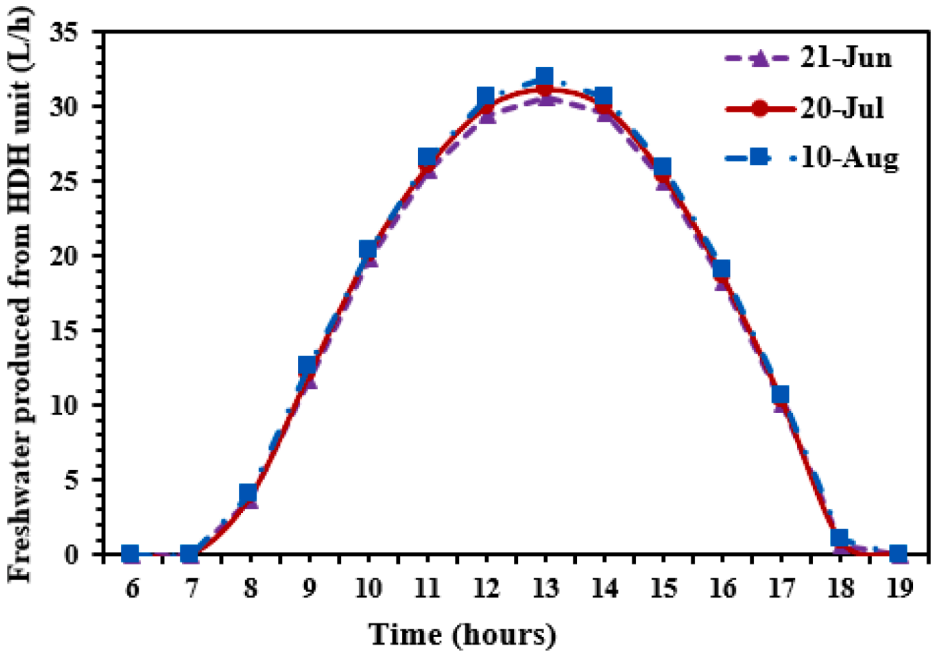


**Fig. 11.** The instantaneous hourly freshwater production from the HDH desalination unit for three different days.

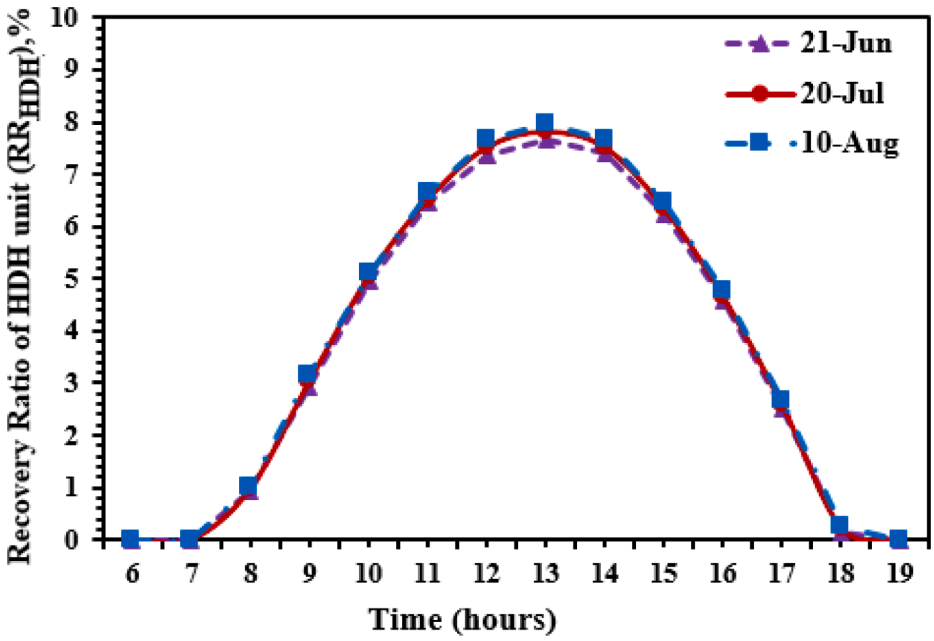


**Fig. 12.** The recovery ratio of the HDH desalination unit for the three different days.

recorded values during each day followed the ordinary trend, i.e., increasing from sunrise till peak at noon and further declination till zero at sunset. The peak values of solar radiation intensities were 1010, 1040, and 1030 W/m$^2$ at solar noon for 21 June, 20 July, and 10 August, respectively. The results of the simulation study of the PV output power on those days are shown in Fig. 10. As noticed, the output power values followed the same of the radiation intensity variation, with the peak of 325, 340, 350 W for 21 June, 20 July, and 10 August, respectively. These values were sufficient to drive the high-pressure pump and air blower of the HDH-RO hybrid system. The DC drive was utilized to control the speed of the high-pressure pump and air blower. In this study, the Pearson pump was being used to adjusted the working pressure to change the feed flow rate.

Fig. 11 demonstrates the instantaneous variations of freshwater production from the HDH desalination unit during three different days. Two SACs and two evacuated tube SWCs was utilized as the thermal energy sources (water to air flow rate ratio = 0.5) in the HDH desalination unit to improve the evaporation rate inside the humidifier. The feed seawater was preheated first in the PV channel and the evacuated tube solar collector before entering the humidifier to increase the evaporation rate. Besides, the air was preheated in the SACs before entering the humidifier to improve its ability to hold more vapor. As seen in Fig. 10, freshwater production from the HDH desalination unit began at the sunrise from zero and increased gradually, reaching peak values of 30.6, 31.2, and 31.9 L/h at solar noon for 21 June, 20 July, and 10 August, respectively, and then gradually declined to zero at sunset.

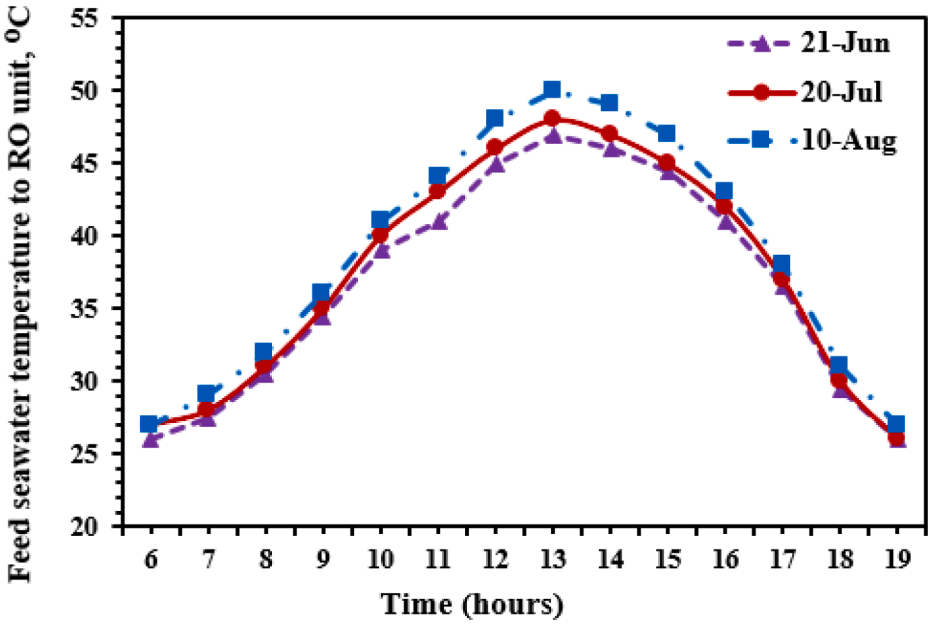


**Fig. 13.** Instantaneous variations of seawater temperature leaving the humidifier and entering the RO desalination unit.

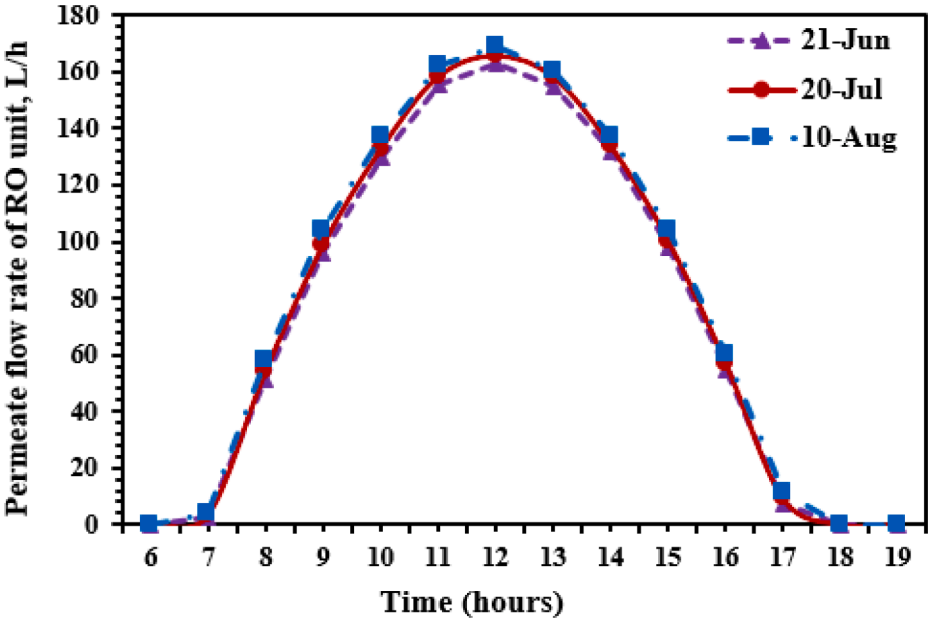


**Fig. 14.** The instantaneous permeate flow rate of the RO desalination unit for three different days.

As shown in Fig. 12, the recovery ratio of the HDH desalination unit reached to 7.7, 7.8, and 8% at solar noon for 21 June, 20 July, and 10 August, respectively.

Fig. 13 demonstrates the instantaneous temperature variations of seawater leaving the humidifier and entering to the RO desalination unit during three different days. As seen, the temperatures varied, similar to solar intensities, from the sunrise with ambient seawater temperature, reaching peak values of 47, 48, 50 °C at solar noon for 21 June, 20 July, and 10 August, respectively, and then declined to same as ambient seawater at sunset.

The permeate flow rates of the RO desalination unit driving by PV panels for three different days are presented in Fig. 14. The presented profiles of the permeate flow rate had the same trend of the corresponding PV power presented within Fig. 9. The maximum permeate flow rate reached to 162.7, 165.4, and 168.8 L/h for 21 June, 20 July, and 10 August, respectively. These results reveal that the permeate flow rate is linearly proportional to PV available power. Fig. 15 shows the recovery ratio of RO desalination unit. As shown, it reached to 40.7, 41.3, and 42.2% at solar noon for 21 June, 20 July, and 10 August, respectively.

Fig. 16 demonstrates the instantaneous variations of freshwater production of the proposed hybrid HDH-RO desalination system. The maximum freshwater produced from the proposed hybrid HDH-RO desalination system reached 192, 195.4, and 200 L/h for 21 June, 20 July, and 10 August, respectively, at noon. These results show that the freshwater produced from the proposed hybrid HDH-RO desalination system is linearly proportional to the PV available power. These results presented that the proposed hybrid HDH-RO desalination system can be a good choice for achieving the highest freshwater production rate compared to the case where both the RO desalination system or the HDH

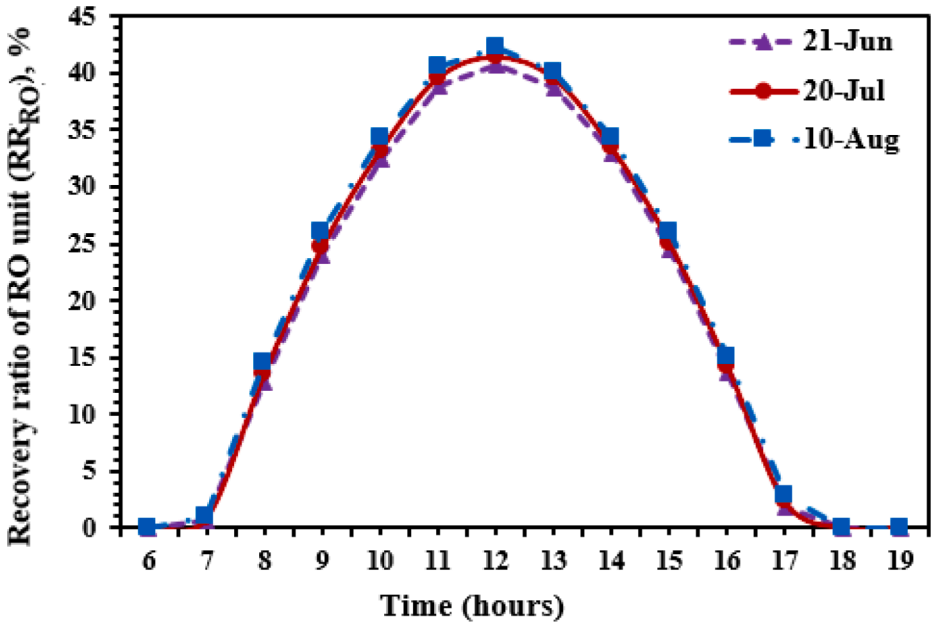


**Fig. 15.** The recovery ratio of the RO desalination unit for the three different days.

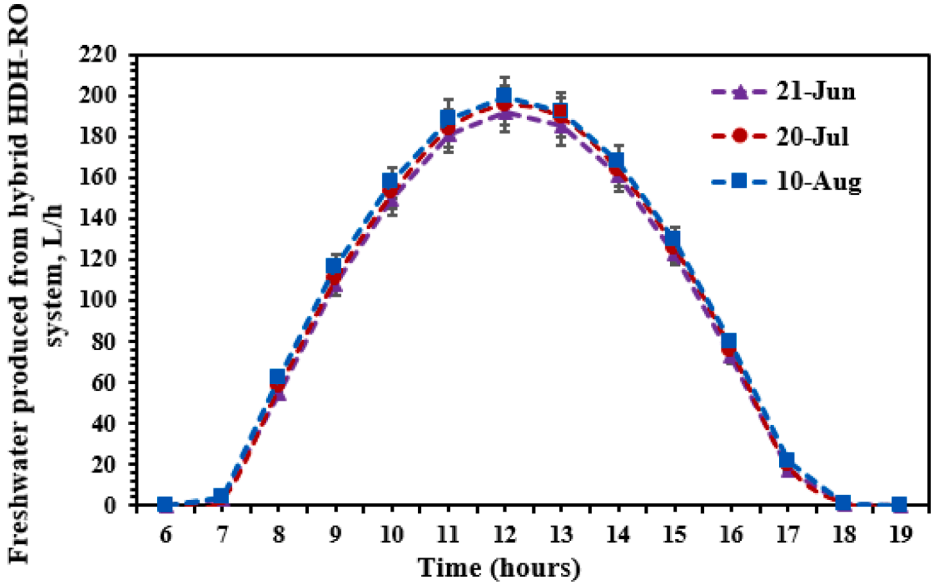


**Fig. 16.** The instantenous variations of freshwater production of the proposed hybrid HDH-RO desalination system.

desalination system are operated separately. On average, the accumulated productivity reached 1284 L/day. Fig. 17 shows the instantaneous variations of the recovery ratio of the proposed hybrid HDH-RO desalination system for the three days. The recovery ratio of the proposed hybrid HDH-RO desalination system had peak values of 48, 48.8, and 49.8% at solar noon for 21 June, 20 July, and 10 August, respectively, at noon.

Table 1 shows the comparison between the specific power consumption (SPC) and freshwater production of the proposed hybrid HDH-RO desalination system in present study with the previous techniques of the RO desalination system. As noticed, the hybrid HDH-RO desalination system proposed in this study is an excellent choice to achieve high freshwater productivity and low SPC compared to previous studies. The specific power consumption (SPC) of the proposed hybrid HDH-RO desalination system ranged between 1.22 and 1.24 kWh/$m^3$, with an average saving a range between 14.7 and 65% compared to the previous techniques of RO desalination system.

## 6. Conclusions

In the present study, a comprehensive performance modeling of a new PV-driven hybrid humidification-dehumidification-reverse osmosis (HDH-RO) desalination system was conducted. The system was provided with thermal energy recovery unit attached to the backside of the PV panels to cool the panels and simultaneously preheat the seawater. In addition, to enhance the evaporation rate within the humidifier, double-pass solar air collectors, and evacuated tube solar water collectors were utilized. For a full analytical assessment of the performance of the proposed unit, five coupled models were suggested, solved, and validated by previously conducted experiments from the literature. The main conclusions of the present simulation study can be reported as follows:

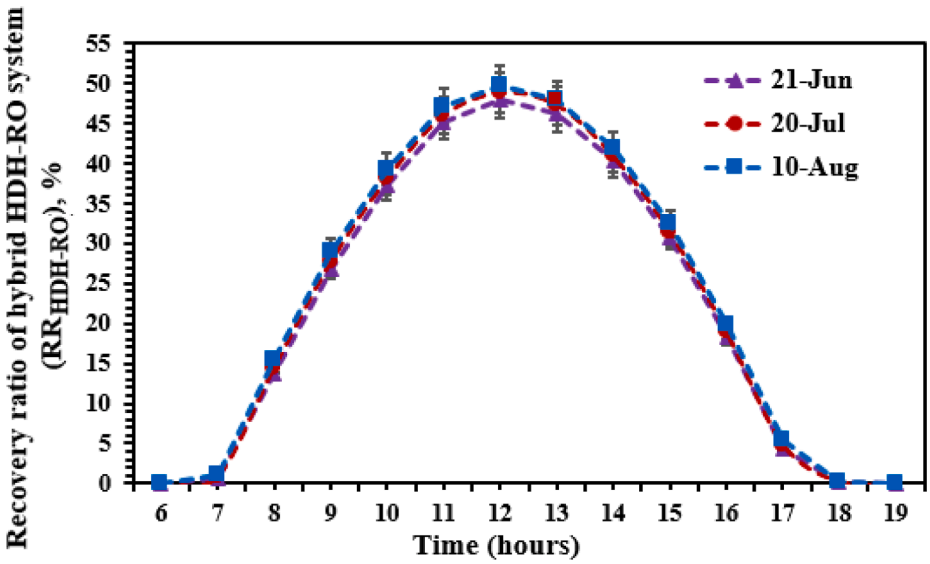


**Fig. 17.** The recovery ratio of the proposed hybrid HDH-RO desalination system.

**Table 1**
Comparison between the specific power consumption of the proposed hybrid HDH-RO system and previous studies.

| Reference | Membrane types | Specific power consumption (SPC), kWh/m$^3$ | |
|---|---|---|---|
| | | Value | Saving ratio in current work (%) |
| Present work | Hybrid HDH-RO with three stage of spiral wound membranes | 1.22–1.24 | – |
| Wang et al. [23] | RO-PRO hybrid system with double ERD | 1.27–1.57 | 15.4 |
| Bargiacchi et al. [25] | hybrid RO-Pressure Retarded Osmosis desalination plants | 1.831–2.227 | 65 |
| Ahmad et al. [26] | Spiral wound membrane (Dow chemical, SW30-4040) in the RO system. | 2–2.14 | 68.3 |
| Cerva et al. [27] | Spiral wound membrane (SW30XHR-440i) in the RO system. | 1.8 | 46.3 |
| Alsarayreh et al. [28] | Spiral wound membrane (Filmtec8I"SW30HR380) in the RO system. | 1.4–2.2 | 46.3 |
| Du et al. [40] | Spiral wound membrane (SW30XLE-400) in the RO system | 1.4107 | 14.7 |
| Avlonitis et al. [41] | Spiral wound membrane (Filmtec8I″SW30HR380) in the RO system | 1.9419 | 57.9 |
| Geraldes et al. [42] | Spiral wound membrane (FilmTec SW30HR-380) in the RO system. | 1.8966 | 54.4 |
| Kaghazchi et al. [43] | Spiral wound membrane (FILMTEC SW30HR-380) in the RO system. | 1.5706 | 27.7 |

- Freshwater production from the HDH desalination unit varied between 30.6 and 31.9 L/h, with a water recovery ratio ranged between 7.7 and 8%.
- The permeate flow rate of RO desalination system ranged between 162.7 and 168.8 L/h, with a water recovery ratio range of 40.7–42.2%.
- The new hybrid HDH-RO desalination system is a good choice for freshwater production with low power consumption.
- The freshwater production of the proposed system varied between192 and 200 L/h, with the water recovery ratio ranged between 48 and 49.8%.
- The specific power consumption (SPC) of this system ranged between 1.22 and 1.24 kWh/m$^3$, with an average saving a range between 14.7 and 65% compared to the previous techniques of RO desalination system.

## CRediT authorship contribution statement

**Mohamed Abdelgaied:** Software, Conceptualization, Resources, Visualization, Formal analysis, Data curation, Validation, Writing - original draft, Writing - review & editing. **A.E. Kabeel:** Formal analysis, Writing - review & editing, Visualization, Supervision, Funding acquisition, Project administration. **A.W. Kandeal:** Resources, Writing - original draft, Writing - review & editing. **H.F. Abosheiasha:** Validation, Writing - review & editing, Visualization, Funding acquisition. **S. M. Shalaby:** Validation, Writing - review & editing, Visualization, Supervision. **Mofreh H. Hamed:** Writing - review & editing, Visualization, Supervision, Project administration. **Nuo Yang:** Software, Formal analysis, Funding acquisition. **Swellam W. Sharshir:** Software, Conceptualization, Resources, Writing - original draft, Writing - review & editing, Formal analysis, Data curation, Validation.

## Declaration of Competing Interest

The authors declare that they have no known competing financial interests or personal relationships that could have appeared to influence the work reported in this paper.

## Acknowledgments

This paper is based upon work supported by Science, Technology & Innovation Funding Authority (STIFA), Egypt and China, under grant (40517). Also, the work was sponsored by National Key Research and Development Project of China (2018YFE0127800) and Fundamental Research Funds for the Central Universities (2019kfyRCPY045). And National Natural Science Foundation of China (51950410592), The authors thank the National Supercomputing Center in Tianjin (NSCC-TJ) and China Scientific Computing Grid (ScGrid) for providing assistance in computations.

## References


[1] Nafey AS, Fath HES, El-Helaby SO, Soliman AM. Solar desalination using humidification dehumidification processes. Part I. A numerical investigation. Energy Convers Manage 2004;45:1243–61.
[2] Mirabdolah Lavasani A, Namdar Baboli Z, Zamanizadeh M, Zareh M. Experimental study on the thermal performance of mechanical cooling tower with rotational splash type packing. Energy Convers Manage 2014;87:530–8.
[3] Zubair MI, Al-Sulaiman FA, Antar MA, Al-Dini SA, Ibrahim NI. Performance and cost assessment of solar driven humidification dehumidification desalination system. Energy Convers Manage 2017;132:28–39.
[4] Rajaseenivasan T, Srithar K. Potential of a dual purpose solar collector on humidification dehumidification desalination system. Desalination 2017;404:35–40.
[5] Ghalavand Y, Rahimi A, Hatamipour MS. Mathematical modeling for humidifier performance in a compression desalination system: Insulation effects. Desalination 2018;433:48–55.
[6] Hooshmand P, Shafii MB, Roshandel R. An experimental study of a solar hybrid system to produce freshwater from waste heat of photovoltaic module by using thermosyphon heat pipes. Energy Convers Manage 2018;158:9–22.
[7] Liu B, Wang C, Bazri S, Badruddin IA, Orooji Y, Saeidi S, et al. Optical properties and thermal stability evaluation of solar absorbers enhanced by nanostructured selective coating films. Powder Technol 2021;377:939–57.
[8] Nižetić S, Čoko D, Yadav A, Grubišić-Čabo F. Water spray cooling technique applied on a photovoltaic panel: The performance response. Energy Convers Manage 2016;108:287–96.
[9] Wang J-H, Gao N-Y, Deng Y, Li Y-L. Solar power-driven humidification–dehumidification (HDH) process for desalination of brackish water. Desalination 2012;305:17–23.
[10] Giwa A, Fath H, Hasan SW. Humidification–dehumidification desalination process driven by photovoltaic thermal energy recovery (PV-HDH) for small-scale sustainable water and power production. Desalination 2016;377:163–71.
[11] Gabrielli P, Gazzani M, Novati N, Sutter L, Simonetti R, Molinaroli L, et al. Combined water desalination and electricity generation through a humidification-dehumidification process integrated with photovoltaic-thermal modules: design, performance analysis and techno-economic assessment. Energy Convers Manage: X 2019;1:100004.
[12] Mohamed AMI, El-Minshawy NA. Theoretical investigation of solar humidification–dehumidification desalination system using parabolic trough concentrators. Energy Convers Manage 2011;52:3112–9.
[13] Rafiei A, Alsagri AS, Mahadzir S, Loni R, Najafi G, Kasaeian A. Thermal analysis of a hybrid solar desalination system using various shapes of cavity receiver: cubical, cylindrical, and hemispherical. Energy Convers Manage 2019;198:111861.
[14] Mahmoud A, Fath H, Ahmed M. Enhancing the performance of a solar driven hybrid solar still/humidification-dehumidification desalination system integrated with solar concentrator and photovoltaic panels. Desalination 2018;430:165–79.
[15] Arefi-Oskoui S, Khataee A, Safarpour M, Orooji Y, Vatanpour V. A review on the applications of ultrasonic technology in membrane bioreactors. Ultrason Sonochem 2019;58:104633.
[16] Alsarayreh AA, Al-Obaidi MA, Al-Hroub AM, Patel R, Mujtaba IM. Evaluation and minimisation of energy consumption in a medium-scale reverse osmosis brackish water desalination plant. J Cleaner Prod 2020;248:119220.
[17] Kotb KM, Elkadeem MR, Khalil A, Imam SM, Hamada MA, Sharshir SW, et al. A fuzzy decision-making model for optimal design of solar, wind, diesel-based RO desalination integrating flow-battery and pumped-hydro storage: case study in Baltim, Egypt. Energy Convers Manage 2021;235:113962.
[18] Ali A, Tufa RA, Macedonio F, Curcio E, Drioli E. Membrane technology in renewable-energy-driven desalination. Renew Sustain Energy Rev 2018;81:1–21.
[19] Elkadeem MR, Kotb KM, Elmaadawy K, Ullah Z, Elmolla E, Liu B, et al. Feasibility analysis and optimization of an energy-water-heat nexus supplied by an autonomous hybrid renewable power generation system: an empirical study on airport facilities. Desalination 2021;504:114952.
[20] Almuhanna EA. Evaluation of single slop solar still integrated with evaporative cooling system for brackish water desalination. J Agric Sci 2014;6:48.
[21] Touati K, Salamanca J, Tadeo F, Elfil H. Energy recovery from two-stage SWRO plant using PRO without external freshwater feed stream: theoretical analysis. Renewable Energy 2017;105:84–95.
[22] Altaee A, Millar GJ, Zaragoza G. Integration and optimization of pressure retarded osmosis with reverse osmosis for power generation and high efficiency desalination. Energy 2016;103:110–8.
[23] Wang Q, Zhou Z, Li J, Tang Q, Hu Y. Investigation of the reduced specific energy consumption of the RO-PRO hybrid system based on temperature-enhanced pressure retarded osmosis. J Membr Sci 2019;581:439–52.
[24] Karimi L, Abkar L, Aghajani M, Ghassemi A. Technical feasibility comparison of off-grid PV-EDR and PV-RO desalination systems via their energy consumption. Sep Purif Technol 2015;151:82–94.
[25] Bargiacchi E, Orciuolo F, Ferrari L, Desideri U. Use of pressure-retarded-osmosis to reduce reverse osmosis energy consumption by exploiting hypersaline flows. Energy 2020;211:118969.
[26] Ahmad N, Sheikh AK, Gandhidasan P, Elshafie M. Modeling, simulation and performance evaluation of a community scale PVRO water desalination system operated by fixed and tracking PV panels: a case study for Dhahran city, Saudi Arabia. Renewable Energy 2015;75:433–47.
[27] La Cerva M, Gurreri L, Cipollina A, Tamburini A, Ciofalo M, Micale G. Modelling and cost analysis of hybrid systems for seawater desalination: electromembrane pre-treatments for reverse osmosis. Desalination 2019;467:175–95.
[28] Alsarayreh AA, Al-Obaidi MA, Farag SK, Patel R, Mujtaba IM. Performance evaluation of a medium-scale industrial reverse osmosis brackish water desalination plant with different brands of membranes. A simulation study. Desalination 2021;503:114927.
[29] Razmjou A, Eshaghi G, Orooji Y, Hosseini E, Korayem AH, Mohagheghian F, et al. Lithium ion-selective membrane with 2D subnanometer channels. Water Res 2019;159:313–23.
[30] Kabeel AE, Khalil A, Elsayed SS, Alatyar AM. Modified mathematical model for evaluating the performance of water-in-glass evacuated tube solar collector considering tube shading effect. Energy 2015;89:24–34.
[31] Du B, Lund PD, Wang J. Combining CFD and artificial neural network techniques to predict the thermal performance of all-glass straight evacuated tube solar collector. Energy 2021;220:119713.
[32] Rani P, Tripathy PP. Thermal characteristics of a flat plate solar collector: Influence of air mass flow rate and correlation analysis among process parameters. Sol Energy 2020;211:464–77.
[33] Vengadesan E, Senthil R. A review on recent developments in thermal performance enhancement methods of flat plate solar air collector. Renew Sustain Energy Rev 2020;134:110315.
[34] Ammar M, Mokni A, Mhiri H, Bournot P. Numerical analysis of solar air collector provided with rows of rectangular fins. Energy Rep 2020;6:3412–24.
[35] Elsafi AM. Integration of humidification-dehumidification desalination and concentrated photovoltaic-thermal collectors: Energy and exergy-costing analysis. Desalination 2017;424:17–26.
[36] Kabeel AE, Abdelgaied M, Sathyamurthy R. A comprehensive investigation of the optimization cooling technique for improving the performance of PV module with reflectors under Egyptian conditions. Sol Energy 2019;186:257–63.
[37] Kabeel AE, Abdelgaied M, Elrefay MKM. Thermal performance improvement of the modified evacuated U-tube solar collector using hybrid storage materials and low-cost concentrators. J Storage Mater 2020;29:101394.
[38] Kabeel AE, Abdelgaied M. Experimental evaluation of a two-stage indirect solar dryer with reheating coupled with HDH desalination system for remote areas. Desalination 2018;425:22–9.
[39] Sharshir SW, Peng G, Elsheikh AH, Edreis EMA, Eltawil MA, Abdelhamid T, et al. Energy and exergy analysis of solar stills with micro/nano particles: A comparative study. Energy Convers Manage 2018;177:363–75.
[40] Du Y, Xie L, Wang Y, Xu Y, Wang S. Optimization of reverse osmosis networks with spiral-wound modules. Ind Eng Chem Res 2012;51:11764–77.
[41] Avlonitis SA, Pappas M, Moutesidis K. A unified model for the detailed investigation of membrane modules and RO plants performance. Desalination 2007;203:218–28.
[42] Geraldes V, Pereira NE, Norberta de Pinho M. Simulation and optimization of medium-sized seawater reverse osmosis processes with spiral-wound modules. Ind Eng Chem Res 2005;44:1897–905.
[43] Kaghazchi T, Mehri M, Ravanchi MT, Kargari A. A mathematical modeling of two industrial seawater desalination plants in the Persian Gulf region. Desalination 2010;252:135–42.